



ENGINEERING SCIENCES

Diclofenac sodium adsorption on activated carbon: experimental, modeling and bayesian statistics

CAMILA S. DIAS, MARCELA ANDREA E. FRANCO, EMERSON C. RODRIGUES, JOSIEL L. FERREIRA, BRUNO M. VIEGAS, LILIANA A. FÉRIS, DIEGO C. ESTUMANO & EMANUEL N. MACÊDO

Abstract: The present study modeled the adsorption process of the drug diclofenac sodium on activated charcoal. For this purpose, a mass balance-based model was used considering a fixed bed column. The mass transfer rate in the solid phase was represented by a driving force model proposed in this study, and a gamma exponent with a range of $0 > \gamma \leq 2$ was assigned to the model. Different isotherms were adopted to represent the equilibrium at the solid/liquid interface: the Langmuir, Freundlich, Sips and Redlich-Peterson isotherms. The modeling was approached from the perspective of Bayesian statistics, and the Markov chain Monte Carlo method was used for parameter estimation. Model validation was performed with experimental data obtained under different operating conditions of initial concentration (C_0), adsorbent mass (W) and feed rate (Q). C_0 and Q were the ones that most influenced the increase in the amount of diclofenac adsorbed on the column. Model selection was performed using the Bayesian information criterion, which indicated that the coupling of the model with the Sips isotherm had the highest probability of representing the experimental breakthrough curves. The model was also able to predict different scenarios in which measurement information was not available.

Key words: Adsorption, drugs, diclofenac, modeling, MCMC, parameter estimation.

INTRODUCTION

Adsorption is a separation process based on the transfer of a certain substance in a fluid to a solid surface with adsorbent capacity (Ruthven 1984). Due to its advantageous operational simplicity, effectiveness and cost of implementation (Lv et al. 2021, Tatarchuk et al. 2021, Shamsudin et al. 2021), adsorption has become one of the most widespread alternatives in the effluent treatment scenario for the removal of so-called emerging pollutants (Nadour et al. 2019, Lonappan et al. 2019, Dang et al. 2020, Deemter et al. 2020).

This class of emerging contaminants includes various chemical species, such as personal care products, pesticides, flame retardants, pharmaceuticals and others. However, drugs deserve to be highlighted since their consumption, whether human or veterinary, has been increasing over the years (Mirzaee et al. 2021). There is also the aggravating factor of the generation of hospital and pharmaceutical effluents, which, together with the excretion of part of these substances produced by

consumer organisms, exposes the environment to interaction with the original molecular structure of these compounds and their metabolites (Lonappan et al. 2016, Pereira et al. 2017, Haro et al. 2021).

Diclofenac (DCF) stands out in this panorama as a non-steroidal anti-inflammatory drug widely used in the treatment of pain and inflammation, having reached a worldwide average consumption of 1443 ± 58 t/year (Acuña et al. 2015) and, in Brazil, it is among the 20 most marketed substances and associations in the 2019/2020 period (Agência Nacional de Vigilância Sanitária 2021). Even if this compound is subjected to conventional treatment plants, these do not promote the complete removal of DCF, making it one of the substances frequently detected in bodies of water (Soares et al. 2019, Zhao et al. 2021, Avcu et al. 2021, Li et al. 2021).

Studies have shown worrying effects on kidney and immun (Hoeger et al. 2005), as well as induction of increased mortality rates in crustaceans at concentrations of around mgL^{-1} (Haap et al. 2008, Lonappan et al. 2016), are some consequences of the constant reinsertion and bioaccumulation of diclofenac in the environment (Zhang et al. 2021).

One tool that can expand the scope of application of adsorption is mathematical modeling. This approach makes it possible to predict scenarios even before experiments are performed, in addition to being essential for project design and scale-up (Vera et al. 2021).

Analytical models in the literature, such as those reported by Yoon-Nelson, Thomas and Bohart-Adams, are able to profile an adsorption process operating in a continuous system (Ahmed et al. 2018, Elabadsa et al. 2019, Nunes et al. 2022, Ferreira et al. 2023). Although these models achieve reasonable fits, detailed information regarding the mass transfer rate in the adsorbent phase is limited, and the ability to obtain parameter values is dependent on the experimental breakthrough curve and corresponding operating conditions (Unuabonah et al. 2019, Juela et al. 2021).

In this sense, the aim of this work was to provide a numerical framework for anticipating breakthrough curve (BC) scenarios that are not yet available experimentally, based on BC information that is already available. It also proposed a simplified model with the differential of a gamma exponent γ ($0 > \gamma \leq 2$) capable of facilitating not only the adjustment to the data but also possibly the scale-up stage.

To this end, Bayesian statistics was adopted and the Markov Chain Monte Carlo (MCMC) method was used to estimate parameters and predict scenarios. The modeling approach mentioned above and applied to a system for adsorbing the drug diclofenac onto activated carbon in a fixed-bed column and using the isotherms of Langmuir, Freundlich, Sips and Redlich-Peterson, to express the equilibrium between the phases has not yet been published in the literature or even in smaller quantities.

The model was validated using experimental data on the adsorption of diclofenac sodium in a fixed-bed column filled with activated carbon. The tests were carried out under different operating conditions of initial concentration C_0 (mg L^{-1}), column feed flow rate Q (ml min^{-1}) and adsorbent mass in the bed W (g).

MATERIALS AND METHODS

Reagents

The experimental solutions were prepared by diluting DCF (analytically pure) supplied by Sigma–Aldrich (St Louis, MO, USA). Granular activated carbon (size fraction between 2.00 and 2.38 mm) was supplied by Êxodo Científica (Hortolândia, SP, Brazil). The adsorbent was washed with water to remove carbon powder and surface impurities, followed by drying at 100 °C for 48 h. The characteristics of the activated carbon were SBET = 462.96 m² g⁻¹ and pHPZC = 6.67.

Analytical method

The DCF concentration of all samples was determined by a UV/Vis spectrophotometer (Thermo Scientific, Genesys 10S UV–Vis) at a wavelength of 276 nm. The samples were filtered prior to analysis.

Fixed bed column experiments

A glass column with an internal diameter of 1.2 cm and a height of 20 cm was used in the fixed bed column adsorption experiments. Layers of high-permeability sintered glass were inserted as supports at the ends of the column. The DCF solution was fed in upflow mode using a peristaltic pump. The different operating conditions evaluated, including the initial concentration of DCF in solution (C_0), feed rate (Q), activated carbon mass (W), height (h) and bed volume (V_L), are shown in Table I.

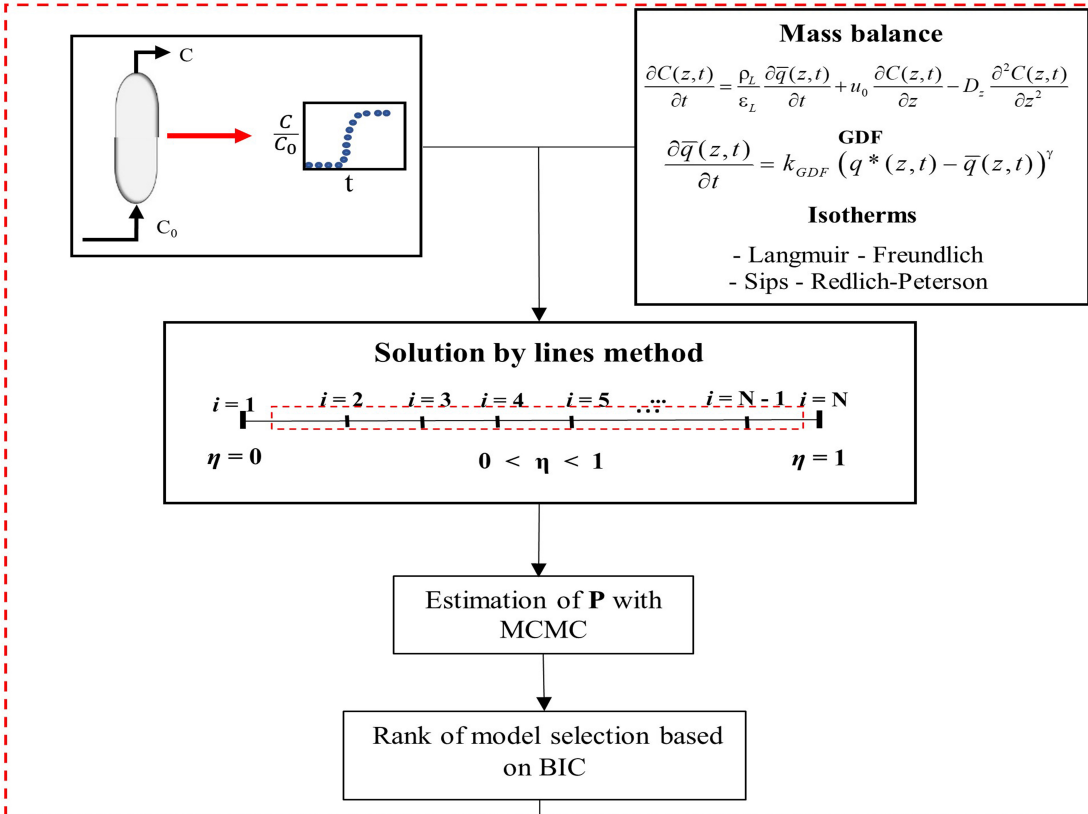
Table I. Operational parameters used in the fixed bed column experiments.

Breakthrough curve	C_0 (mgL ⁻¹)	Q (mLmin ⁻¹)	W (g)	V_L (cm ³)	h (cm)
1	20.00	3.00	0.50	0.57	0.50
2	100.00	3.00	0.50	0.57	0.5
3	20.00	3.00	1.50	1.70	1.50
4	100.00	3.00	1.50	1.70	1.50
5	20.00	5.00	0.50	0.57	0.50
6	100.00	5.00	0.50	0.57	0.50
7	20.00	5.00	1.50	1.70	1.50
8	100.00	5.00	1.50	1.70	1.50
9	60.00	4.00	1.00	1.13	1.00

Estimation of parameters and predictions

Fig. 1 presents the structure and sequential stages of this study. In the first stage, the relevant model parameters were estimated with the Markov chain Monte Carlo (MCMC) method; the fit was assessed,

Step 1



Step 2

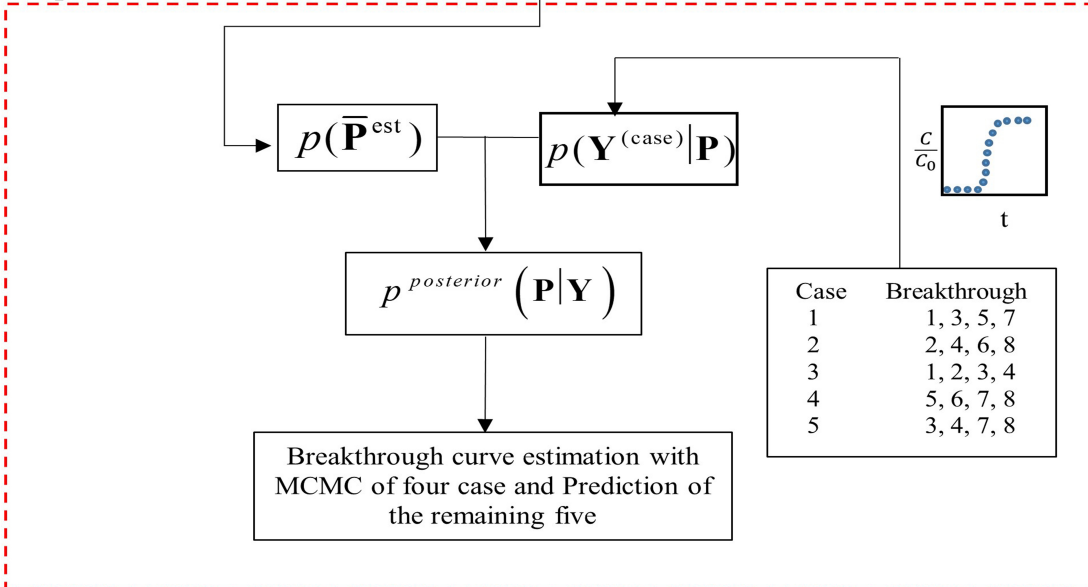


Figure 1. Structure and sequential stages of the present study.

and models were selected on the basis of the adjusted coefficient of determination R_a^2 and the Bayesian information criterion (BIC).

In the second stage, the data from four breakthrough curves were used for the probability $p(\mathbf{Y}^{(case)}|\mathbf{Y})$ grouped according to which operating parameter - C_0 , Q or W - was kept fixed.

The parameters previously estimated in the first stage $p(\bar{\mathbf{P}}^{est})$ were used in the initial distribution of the second stage. From this information, the model was tested for the prediction of the five remaining breakthrough curves, whose experimental data were not used in the likelihood. Table II presents the parameters that were estimated for each model/isotherm coupling and their initial values.

Table II. Vector of estimated parameters.

	Isotherm	Estimated parameters
Mass balance model + GDF	Langmuir	$\mathbf{P} = [k_s \gamma k_L]$
	Freundlich	$\mathbf{P} = [k_s \gamma k_F n]$
	Sips	$\mathbf{P} = [k_s \gamma k_{Sips} \beta]$
	Redlich-Peterson	$\mathbf{P} = [k_s \gamma k_{RP} a_{RP} b]$

Fig. 2 shows the MCMC method implementation according to the Metropolis-Hastings algorithm wherein RH refers to the Hastings ratio, used as the accept-reject algorithm. A uniform probability distribution $U[0, 10P^{Ref}]$ was adopted with a minimum value of zero and a maximum value ten times the reference, P^{Ref} . The data obtained in this study were assumed to be normally distributed, and an experimental uncertainty of 1% was considered acceptable.

Candidate parameters were generated by means of a perturbation around the immediately previous parameter according to Equation 1.

$$\mathbf{P}^* = \mathbf{P}^{-1} + \mathbf{P}^{i-1} w r_N \quad (1)$$

where w is the search step, with a value of 0.003. r_N represents a random number from the normal distribution.

The method of lines was applied to solve the general mass balance model, reducing it to a set of differential equations in time by means of discretization in η space (Shakeri & Dehghan 2008), where the interval $0 < \eta < 1$ corresponds to the internal points of the mesh. It is noteworthy that the experimental measurements were collected at the exit of the column, i.e., when $\eta = 1$.

To avoid possible interference from different orders of magnitude on the parameter estimation process (Otálvaro-Marín & Machuca-Martínez 2021, Huang et al. 2022), the dimensionless versions of Equations 2 and 5-13 were used.

MATHEMATICAL MODELING OF THE ADSORPTION COLUMN

The mathematical model of the fixed bed adsorption column was established from a mass balance. The simplifying assumptions of the model considered here were as follows: constant axial dispersion

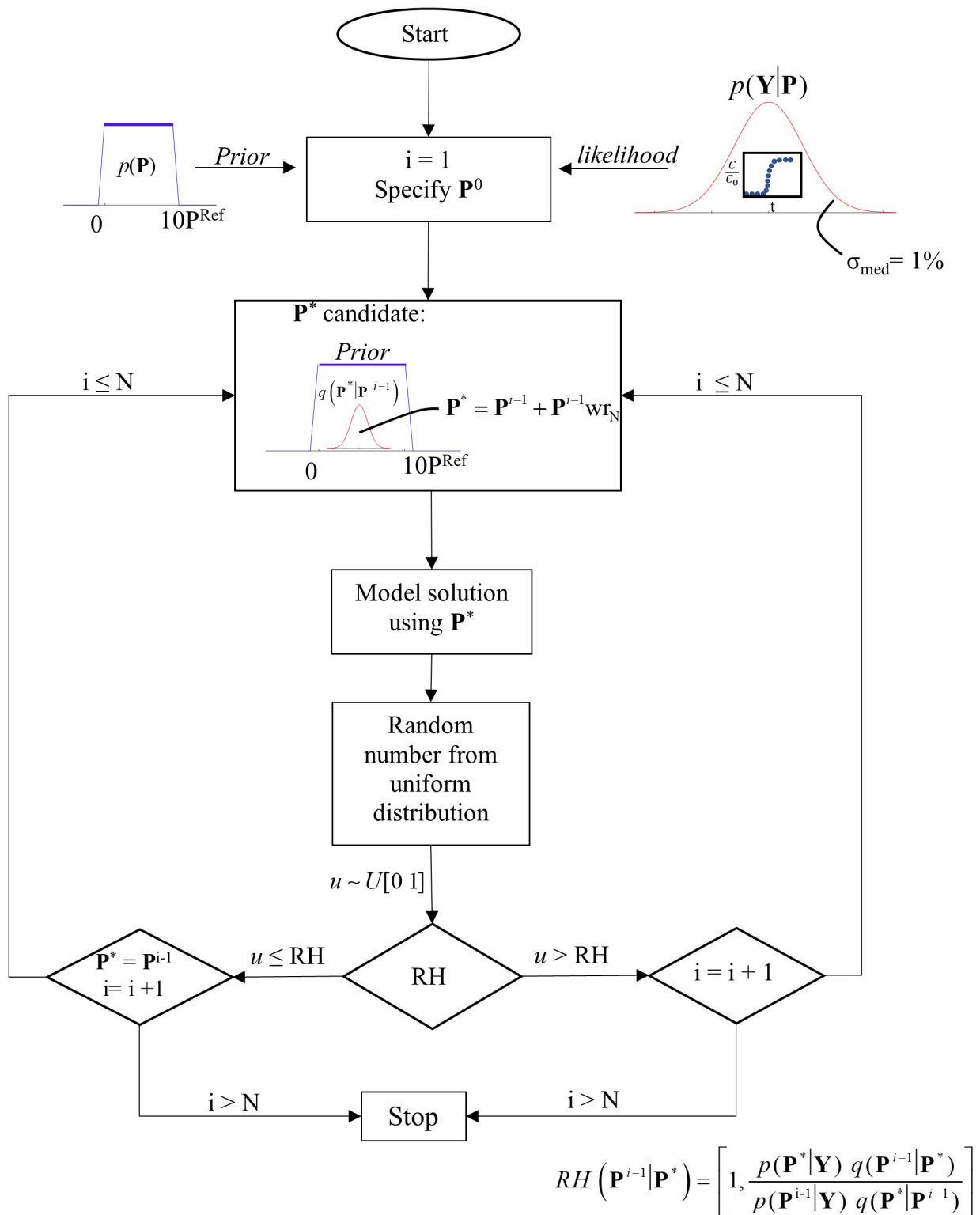


Figure 2. MCMC method implementation according to the Metropolis-Hastings algorithm.

and porosity, mass flow significant only in the axial direction, and the solid/liquid interface as the condition of thermodynamic equilibrium (Módenes et al. 2021). Such hypotheses are well accepted in the literature for this type of problem. The balance sheet equation takes the form shown by Equation 2.

$$\frac{\partial C(z, t)}{\partial t} = \frac{\rho_L}{\epsilon_L} \frac{\partial \bar{q}(z, t)}{\partial t} + u_0 \frac{\partial C(z, t)}{\partial z} - D_z \frac{\partial^2 C(z, t)}{\partial z^2} \quad (2)$$

With $0 < z < L, t > 0$.

The term on the left hand-side of Equation 2 represents the rate of change in DCF in the liquid phase. The first term on the right refers to the rate of change of solute in the adsorbent solid phase, and the second and third terms on the right correspond to the convective and diffusive effects, respectively. C and q are the DCF concentrations in the liquid phase (mg L^{-1}) and in the solid phase (mg g^{-1}), respectively, ϵ_L is the porosity of the bed, ρ_L is the bed specific gravity (g L^{-1}), D_z is the axial dispersion ($\text{cm}^2 \text{min}^{-1}$) and u_0 is the interstitial velocity (cm min^{-1}).

Rate equation in the adsorbent phase

The term in Equation 2 that represents the rate of change of solute in the solid phase, $\partial \bar{q}(z, t)/\partial t$, is often represented in the literature by the linear driving force (LDF) model (Equation 3). The LDF considers an average value (\bar{q}) for the adsorbate concentration in the solid phase, as shown in Fig. 3, and its difference relative to the equilibrium condition at the interface (q^*) is proportional to the mass transfer rate in the adsorbent. This kinetic model describes adsorption on the solid surface as a mechanism of mass transfer and assumes that the particles are a homogeneous phase and that the reaction kinetics are much faster than the mass transfer steps (Scheufele et al. 2021).

$$\frac{\partial \bar{q}(z, t)}{\partial t} = k_s(q^*(z, t) - \bar{q}(z, t)) \quad (3)$$

With $0 < z < L, t > 0$. Where k_s (min^{-1}) is the global mass coefficient.

Another approach to describe the rate of change of solute in the solid phase is given by the quadratic driving force (QDF) model (Equation 4). This model assumes concentration dependence and considers that the mass transfer coefficient is zero at equilibrium (Brandani 2020). k_{QDF} ($\text{mg g}^{-1} \text{min}^{-1}$) is the constant of Equation 4.

$$\frac{\partial \bar{q}(z, t)}{\partial t} = k_s(q^*(z, t) - \bar{q}(z, t))^2 \quad (4)$$

with $0 < z < L, t > 0$.

From Equations 3 and 4, a gamma exponent ($0 < \gamma \leq 2$) was assigned to the rate equation called the gamma driving force (GDF) in this work. The value of this exponent can range over an interval instead of assuming only a fixed value for all cases, with the aim of estimating the best value with respect to goodness of fit. If $\gamma = 1$, Equation 5 tends to the LDF, and if $\gamma = 2$, it will tend to the QDF. The GDF equation is shown in Equation 5; k_{GDF} ($(\text{mg g}^{-1})^{1-\gamma} (\text{min}^{-1})$) is the constant of this equation.

$$\frac{\partial \bar{q}(z, t)}{\partial t} = k_s(q^*(z, t) - \bar{q}(z, t))^\gamma \quad (5)$$

with $0 < z < L, t > 0$.

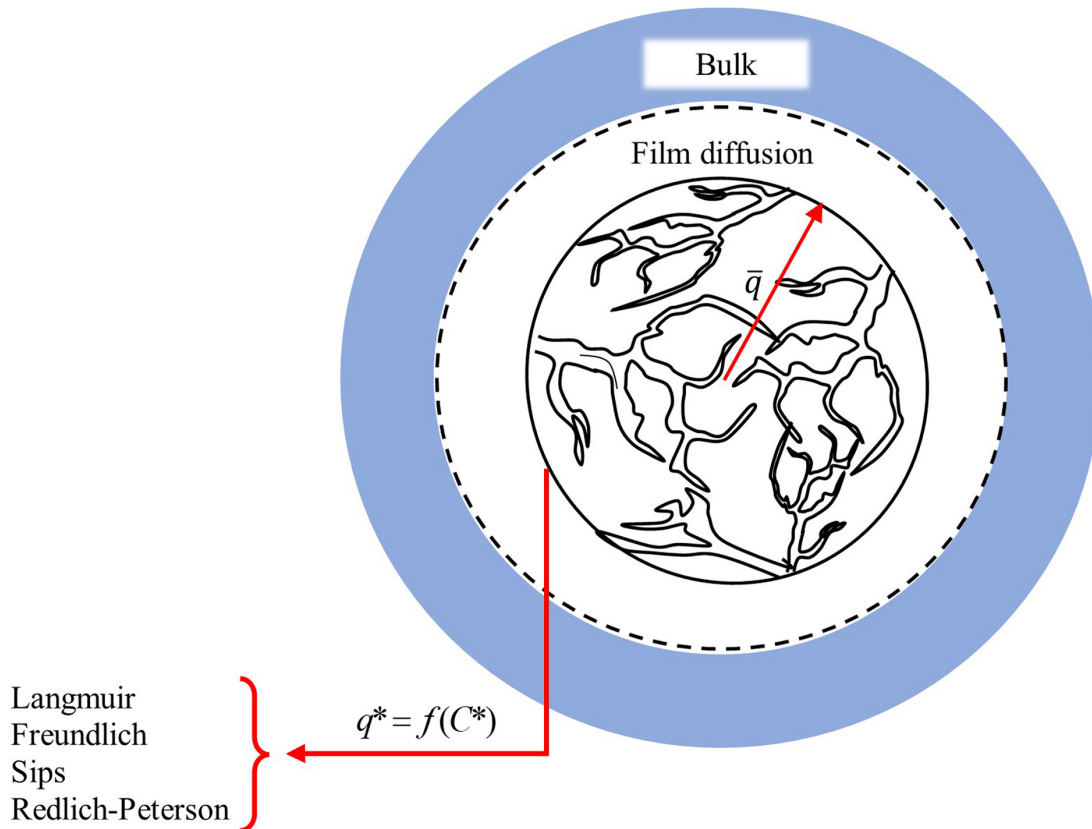


Figure 3. Schematic representation of the equilibrium dynamics in the adsorbent phase and the equilibrium isotherms used.

Equilibrium relationships

The Langmuir, Freundlich, Sips and Redlich-Peterson isotherms were adopted in this study to represent the equilibrium between the liquid and adsorbent phases. The Langmuir isotherm is represented in Equation 6 and considers that adsorption occurs in a monolayer without interactions between the adsorbed molecules.

$$q^* = \frac{q_{max} k_L C_{eq}}{1 + k_L C_{eq}} \quad (6)$$

where q^* (mg g^{-1}) is the amount of solute adsorbed per gram of adsorbent at equilibrium, q_{max} (mg g^{-1}) is the maximum adsorption capacity, k_L (L mg^{-1}) is the Langmuir constant and C_{eq} (mg L^{-1}) is the adsorbate concentration at equilibrium.

The Freundlich isotherm, Equation 7, assumes multilayer adsorption, the possibility of interaction between the adsorbed molecules and solid surface heterogeneity.

$$q^* = k_F C_{eq}^{1/n} \quad (7)$$

where C_{eq} (mg L^{-1}) is the solute concentration at equilibrium, k_F ($(\text{mg g}^{-1})/(\text{L mg}^{-1})^{1/n}$) is the Freundlich constant, which measures the adsorption capacity, $1/n$ is related to surface heterogeneity

and n is a parameter that estimates the intensity of adsorption (Ayawei et al. 2017, Togue Kanga 2019, Okpara et al. 2021, Martins et al. 2020).

The Sips isotherm, Equation 8, is a combination of the Langmuir and Freundlich isotherms, and despite setting a maximum limit for adsorption, it allows the use of high values for the adsorbate concentration. It is used to represent heterogeneous adsorption and, at low concentrations, tends to the Freundlich isotherm. At higher concentrations, it exhibits monolayer behavior similar to the Langmuir isotherm (Saadi et al. 2015, Ayawei et al. 2017, Jemutai-Kimosop et al. 2022, Kalam et al. 2021).

$$q^* = \frac{q_{max} k_{Sips} C_{eq}^\beta}{1 + k_{Sips} C_{eq}^\beta} \quad (8)$$

where q_{max} is the maximum adsorption capacity ($mg\ g^{-1}$), k_{Sips} is the equilibrium constant ($L\ mg^{-1}$), C_{eq} ($mg\ L^{-1}$) is the equilibrium solute concentration and β is the heterogeneity of the system and can range from 0 to 1, where for $\beta = 1$, the system is considered homogeneous, which is equivalent to the Langmuir model, and for $\beta < 1$, it represents increased heterogeneity (Chen et al. 2022).

The Redlich-Peterson isotherm, Equation 9, is also a hybrid between the Langmuir and Freundlich isotherms. It can be applied over a wide range of concentrations and represents both homogeneous and heterogeneous systems without following the traditional monolayer representation (Kalam et al. 2021). At low concentrations, this model tends to the Langmuir isotherm, and at higher concentrations, it tends to the Freundlich isotherm (Wang & Guo 2020).

$$q^* = \frac{k_{RP} C_{eq}}{1 + a_{RP} C_{eq}^b} \quad (9)$$

where k_{RP} ($L\ g^{-1}$) and a_{RP} ($L^b mg^{-b}$) are the parameters of the Redlich-Peterson isotherm and b is the exponent ($0 \leq b \leq 1$).

The initial conditions used to solve Equation 2 are presented in Equations 10-11.

$$C(z, 0) = 0 \quad (10)$$

$$q(z, 0) = 0 \quad (11)$$

with $0 < z < L$, $t = 0$.

The boundary conditions used are shown in Equations 12-13.

$$-D_{ax} \frac{\partial C(z, t)}{\partial z} = u_0 (C_0 - C(z, t)) \quad (12)$$

with $z = 0$, $t > 0$.

$$-\frac{\partial C(z, t)}{\partial z} = 0 \quad (13)$$

with $z = L$, $t > 0$

In Equation 12, the adsorbate feed rate into the column by diffusion and flow is considered to be constant after it crosses the plane at $z = 0$, where C_0 is the initial adsorbate concentration ($mg\ L^{-1}$). Equation 13 assumes the boundary condition of a constant concentration at the exit of the bed (Danckwerts 1953).

The amount adsorbed until the saturation time, q_{sat} , may represent the maximum capacity of a given adsorbent in a fixed bed column. In this work, Equation 14 was used to obtain the q_{max} of the adsorbent for use in the Sips and Langmuir isotherms (Geankoplis 1993).

$$q^* = q_{max} = \frac{C_0 Q}{1000W} \int_0^{t_f} \left(1 - \frac{C}{C_0}\right) dt \tag{14}$$

where Q is the volumetric flow rate of the bed (mL min^{-1}) and W is the mass of the adsorbent (g).

Fig. 4 schematically illustrates the adsorption column, the differential elements considered for the balance and arrangement of the equations as well as the column region that each equation represents.

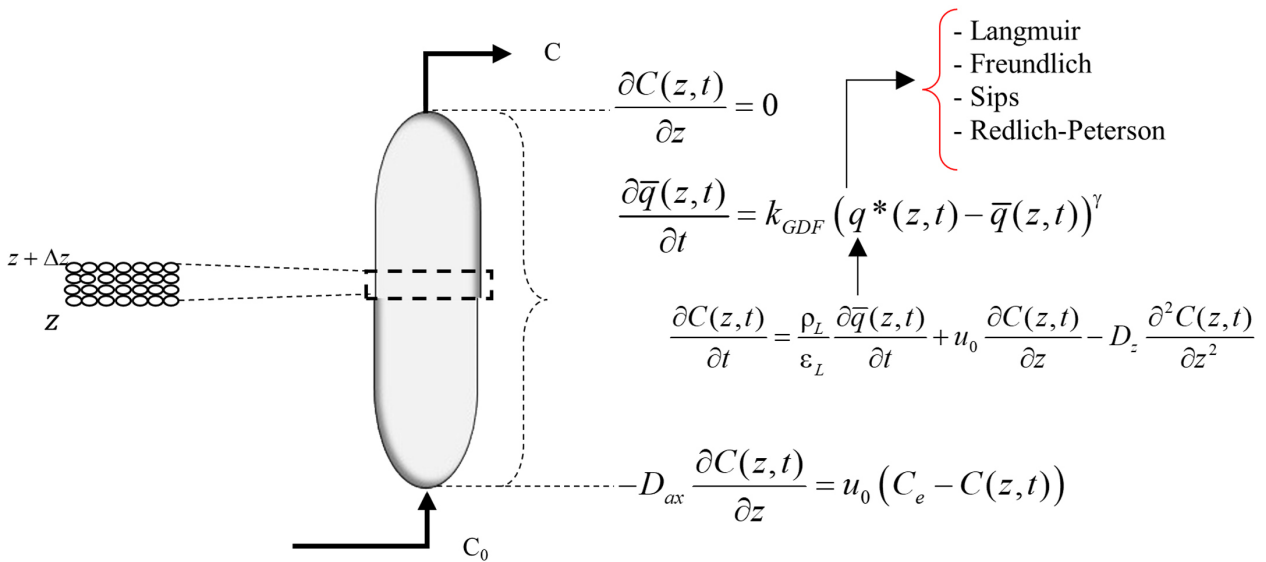


Figure 4. Schematic representation of the adsorption column and the balance equations in each column region.

Bayesian inference

Bayesian inference allows the use of information available prior to the beginning of the process, which is included in the a priori probability distribution of the parameters $p(\mathbf{P})$, and the information from the experimental measurements is included in the probability $p(\mathbf{Y}|\mathbf{P})$. The combination of these sets of information provides the posterior probability distribution $p(\mathbf{P}|\mathbf{Y})$.

Bayes' theorem, shown in Equation 15, presents the formal arrangement of these distributions (Kaipio & Somersalo 2004); $p(\mathbf{Y})$ is the marginal probability distribution of the measurements serves only as a normalization constant (Moura et al. 2021, 2022, Amador et al. 2022, Tavares et al. 2022, Jurado-Davila et al. 2023a, b, Nunes et al. 2021, Viegas et al. 2023, Cardoso et al. 2023).

$$p(\mathbf{P}|\mathbf{Y}) = \frac{p(\mathbf{P})p(\mathbf{Y}|\mathbf{P})}{p(\mathbf{Y})} \propto p(\mathbf{P})p(\mathbf{Y}|\mathbf{P}) \tag{15}$$

Sampling methods are generally used to obtain samples from the posterior distribution, one of which is the MCMC method. This method is widely adopted in the literature and was implemented in

the present study with the Metropolis–Hastings algorithm. More details on the general structure of this method can be found in Gamerman & Lopes (2006) and in the Materials and Methods section with the adaptations for the present study.

The BIC is used in scenarios involving concurrent models, and the model with the lowest value of this metric is most likely to represent the studied physical phenomenon (Toffoli de Oliveira et al. 2023). In this study, the BIC (Equation 16) was applied to select the appropriate model/isotherm coupling for modeling the adsorption of DCF on a fixed bed of activated carbon.

$$BIC = -2\log[p(\mathbf{Y}|\mathbf{P})] + N_p\log(N_{med}) \quad (16)$$

where N_p represents the number of parameters to be estimated and N_{med} represents the number of measurements used.

RESULTS AND DISCUSSION

Fig. 5 presents the experimental data obtained under different operating conditions, as shown in Table I, for nine tests of DCF adsorption in a fixed bed column with the commercial adsorbent activated carbon.

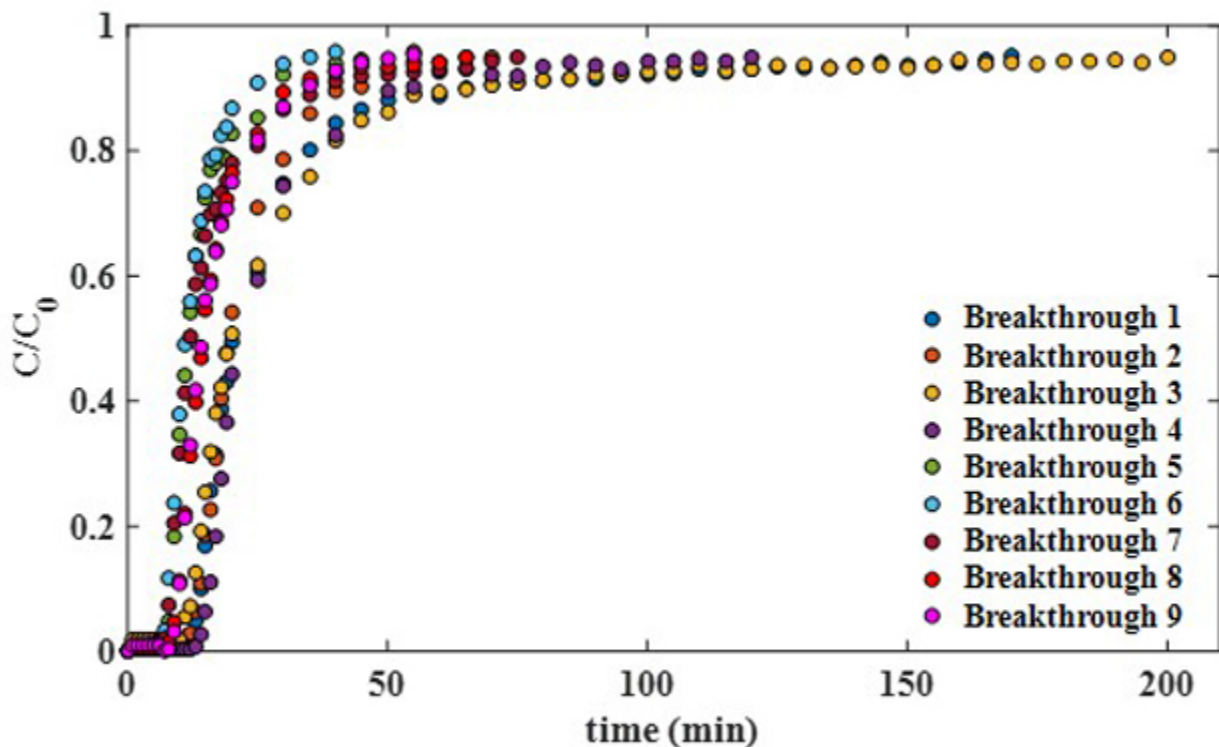


Figure 5. Breakthrough curves obtained under different experimental conditions.

Table III compares the results of the maximum adsorption capacity q_{max} found in the literature for different types of adsorbent materials with the result obtained in the present work for breakthrough curve 2. The results of the other curves can be consulted in the supplementary material and the q_{max} values are in the same order of magnitude.

Table III. q_{max} of the different adsorbents in the literature and breakthrough curve 2.

Adsorbent material	q_{max}	Experimental conditions	References
Biohybrid aerogel	321.3 mg g ⁻¹	Batch adsorption $C_0 = 50 - 800 \text{ mg L}^{-1}$ PH = 5 – 10 $W = 0.2-1.5 \text{ g L}^{-1}$	Tang et al. 2023
Thermo-plasma expanded graphite	433.29 mg g ⁻¹	Batch adsorption $C_0 = 10-250 \text{ mg L}^{-1}$ $W = 10 \text{ mg}$ $V = 50 \text{ mL}$ PH = 1	Cuccarese et al. 2021
Reduced graphene oxide aerogel (rGOA)	596.71 mg g ⁻¹	Batch adsorption $C_0 = 325 \text{ mg L}^{-1}$ $W = 0.25 \text{ g L}^{-1}$	Hiew et al. 2018
Chitosan/fibrous silica KCC-1	142.01 mg g ⁻¹	Batch adsorption $C_0 = 60 \text{ mg L}^{-1}$ $W = 0.15 \text{ g L}^{-1}$ PH = 4	Lai et al. 2023
Composite of heavy polyethylene sugarcane ash and terephthalate (PETSCA/Fe ³⁺)	324.34 μg^{-1}	Fixed bed adsorption $C_0 = 500 \mu\text{g L}^{-1}$ $W = 4 \text{ g}$ $Q = 2 \text{ mL min}^{-1}$	Américo-Pinheiro et al. 2022
Activated carbon	14.73 mg g ⁻¹	Fixed bed adsorption $C_0 = 100 \mu\text{g L}^{-1}$ $W = 0.5 \text{ g}$ $Q = 3 \text{ mL min}^{-1}$	This work

Table III indicates promising results in the development and improvement of adsorbent materials, as can be seen from their high adsorbent capacities. In the present study, granular activated carbon was chosen because it is an effective material with satisfactory performance in the treatment of real water samples (Saarela et al. 2020, da Silva Medeiros et al. 2023), it is ecologically attractive, it has an affinity with various compounds, it has ample sources of raw materials, it is easy to prepare and it

is a viable and economically competitive option compared to other adsorbent materials (Kamarudin et al. 2021, Wu et al. 2019, Amalina et al. 2022, Dong et al. 2023).

The data shown in Fig. 5 were fed into the probability calculation for parameter estimation with the MCMC method. Each experimentally obtained breakthrough curve was evaluated individually with the mass balance model coupled with the Langmuir, Freundlich, Sips and Redlich-Peterson isotherms. The results for these individual estimates are presented in Fig. 6 in a dimensionless scenario, considering a variable DCF concentration at the exit of the column (θ) over time (τ). The dimensionless groups adopted here are available in the supplementary material. In general, the breakthrough curves based on parameter estimation satisfactorily approximated the experimental results.

The estimated curves follow the behavior of the real breakthrough curves, from the region before the breakthrough point and passing through the entire mass transfer zone until reaching the equilibrium region. The number of states of the Markov chain (N) adopted here was 10,000, and this number of states proved to be sufficient to obtain good fits.

The Freundlich model/isotherm combination showed a deviation from the experimental data, especially in the thermodynamic equilibrium region, for the nine breakthrough curves in Fig. 6. The estimated mean value for the parameter n , which represents the deviation from linearity, was 1.5, within a 99% reliability interval, indicating that this is a favorable physical adsorption process because $n > 1$ (Pezoti et al. 2016, Kumar et al. 2018). Regarding the Sips isotherm, the mean estimated value obtained for the β parameter was 0.83, within a 99% reliability interval, indicating a system with increased heterogeneity under the evaluated experimental conditions because $\beta < 1$.

The breakthrough curve estimated using the Langmuir isotherm presented a coherent fit to the experimental data, as seen from the adjusted correlation coefficient of 0.99 and the value of the Bayesian metric BIC (Table IV).

Table IV. Adjusted R^2 and BIC values for the nine breakthrough curves, estimated individually with the model combined with the Langmuir, Freundlich, Sips and Redlich-Peterson isotherms.

Breakthrough curve	Langmuir		Freundlich		Sips		Redlich-Peterson	
	Adjusted R^2	BIC	Adjusted R^2	BIC	Adjusted R^2	BIC	Adjusted R^2	BIC
1	0.99	764.01	0.98	1725.37	0.99	420.58	0.98	1082.93
2	0.99	505.50	0.99	358.50	0.98	488.38	0.99	313.55
3	0.99	818.47	0.98	1717.93	0.99	589.53	0.99	631.58
4	0.99	242.62	0.98	869.31	0.99	309.46	0.99	379.82
5	0.98	469.75	0.98	624.26	0.98	455.18	0.99	294.69
6	0.99	333.65	0.99	233.37	0.98	336.18	0.99	132.04
7	0.99	263.80	0.97	968.52	0.99	240.66	0.99	336.19
8	0.99	282.40	0.99	372.87	0.99	369.59	0.99	199.53
9	0.99	333.55	0.98	440.58	0.98	404.27	0.99	91.49

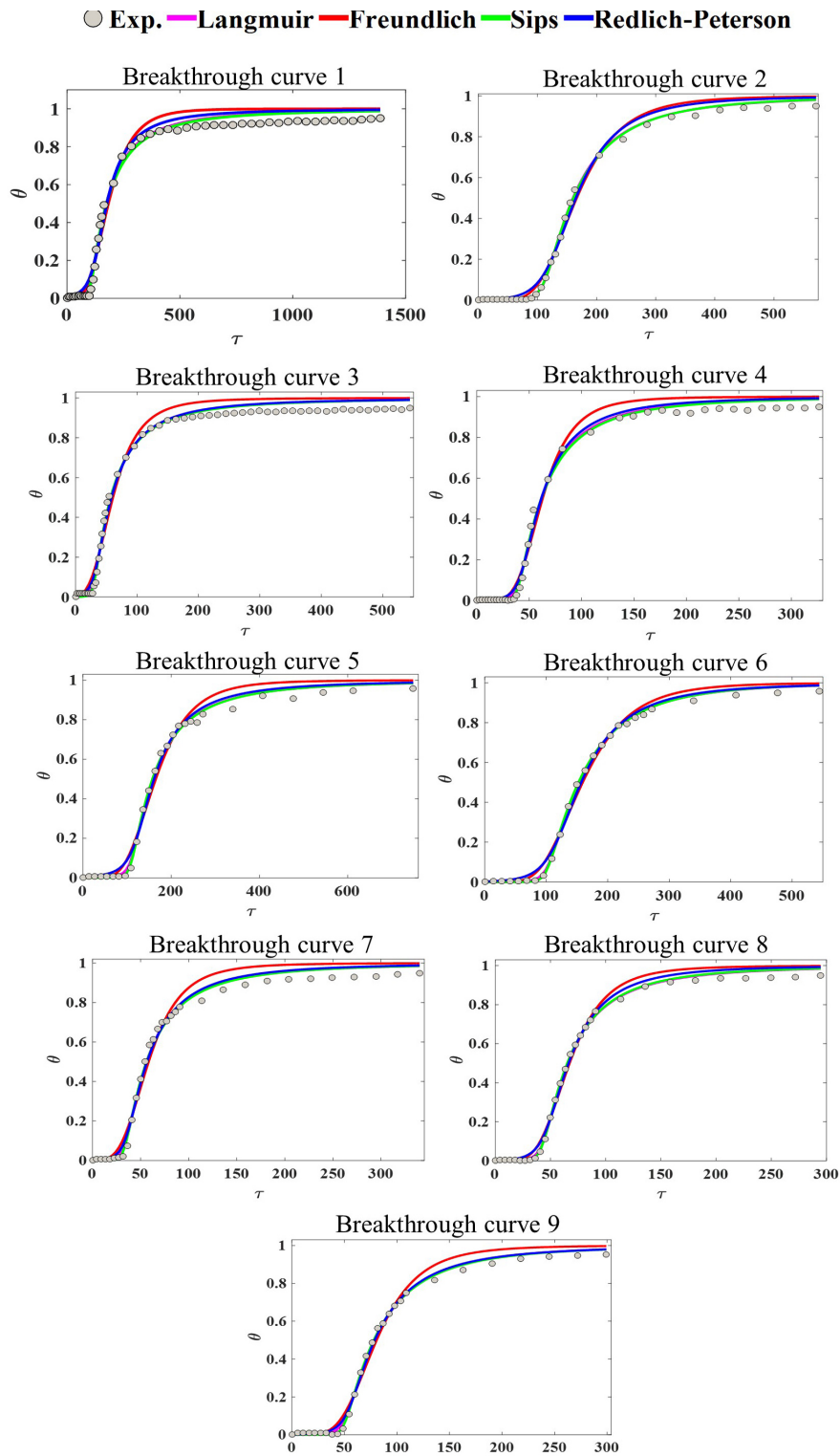


Figure 6. Experimental breakthrough curves and those estimated with the model/GDF/isotherm (Langmuir, Freundlich, Sips or Redlich-Peterson) couplings.

When considering only the adjusted correlation coefficient, in most cases, the Langmuir isotherm presented a result closer to unity than did the Sips isotherm. However, the use of the BIC for model selection enables more thorough analysis of the scenario, as the lower values indicate that the Sips isotherm has the highest probability of representing the physical phenomenon of DCF adsorption on activated carbon. This was the case except for curves 4, 6 and 9, in which the lowest BIC value was obtained for the Langmuir isotherm; it is noteworthy, however, that this difference was small.

The coupling of the Redlich-Peterson isotherm with the mechanistic model adopted here provided a coherent fit to the experimental data, as observed in Fig. 6. The mean value of the parameter b of this isotherm for the nine breakthrough curves was 0.97 within a 99% confidence interval, demonstrating that this equation tends to be equivalent to the Langmuir isotherm because b approximates 1 (Chen et al. 2022). The lowest value of BIC was obtained with this isotherm under the experimental conditions of breakthrough curve 9, which corresponds to the center point conditions.

Table V presents the initial values used for the parameters and the average estimates obtained for each parameter. The Peclet number was the only parameter not subjected to estimation due to the small influence it exerted on the breakthrough curve profile and was kept fixed at $Pe = 30$. The other estimated parameters were within a reliability interval of 99% and can be used as a priori information in further studies on the adsorption of drugs in fixed bed columns.

Table V. Operational parameters used in the fixed bed column experiments.

Reference parameter values									
k_s	k_L	k_F	n	k_{Sips}	β	k_{RP}	a_{RP}	b	Pe
0.05	2.00	100	1.00	2.00	1.00	0.20	1.00	1.00	30.00
Estimated parameter values									
k_s	k_L	k_F	n	k_{Sips}	β	k_{RP}	a_{RP}	b	Pe
0.16	19.64	80.52	1.49	0.17	0.83	0.71	8.27	0.97	30.02

Table VI shows the estimated values for the γ parameter of the GDF equation within a 99% confidence interval. In none of the evaluated cases was the value of this parameter restricted to 1 or 2, which leads to the conclusion that a linear model such as the LDF or even a quadratic model such as the QDF would not be sufficient to represent the kinetics in the adsorbent solid phase.

Thus, this exponent confers greater flexibility, which can result in a better fit to the data due to the possibility of covering values within an interval consistent with information in the literature.

It is noteworthy that, despite the simplicity of the GDF model, it was effective in describing the mass transfer rate in the adsorbent solid phase, which indicated its potential as an alternative to the more complex equations used to describe such dynamics.

Table VI. Value obtained for the gamma exponent of the GDF equation for the nine experimental breakthrough curves.

Breakthrough curve	Gamma driving force parameter			
	Langmuir	Freundlich	Sips	Redlich-Peterson
1	1.99	1.25	1.99	1.93
2	1.52	1.40	1.46	1.51
3	1.99	1.52	1.99	1.98
4	1.64	1.49	1.62	1.62
5	1.78	1.36	1.69	1.89
6	1.31	1.28	1.26	1.53
7	1.86	1.47	1.75	1.74
8	1.61	1.47	1.55	1.44
9	1.46	1.43	1.47	1.61

Breakthrough curve predictions

The mass balance model was evaluated regarding its ability to predict breakthrough curves under different operating conditions. Table VII shows case 1, in which the initial DCF concentration C_0 was kept constant, and breakthrough curves 1, 3, 5 and 7 were used for probability calculations. With this information, the model was tested in the prediction of the five remaining breakthrough curves. The other five cases were evaluated, and their results can be found in the Supplementary Material of this work.

Table VII. Fixed value of the operating parameter C_0 and breakthrough curves used for probability prediction.

Case	Fixed operating parameter	Breakthrough curves used in likelihood			
C_0	20	1	3	5	7

Figs. 7-10 show the predictions obtained with the model coupled to the Langmuir, Freundlich, Sips and Redlich-Peterson isotherms. The graphs present the estimates for the breakthrough curves whose data were used for the probability calculations, as well as the predicted profiles for the remaining five curves.

The model coupled with the Langmuir isotherm, Fig. 7, best represented the breakthrough curves whose experimental data were not used in the probability calculation. Similar performance was observed for the model coupled with the Sips isotherm (Fig. 9), in which only case 1 performed better with the Langmuir isotherm than with the Sips isotherm, as it predicted the data corresponding to curve nine.

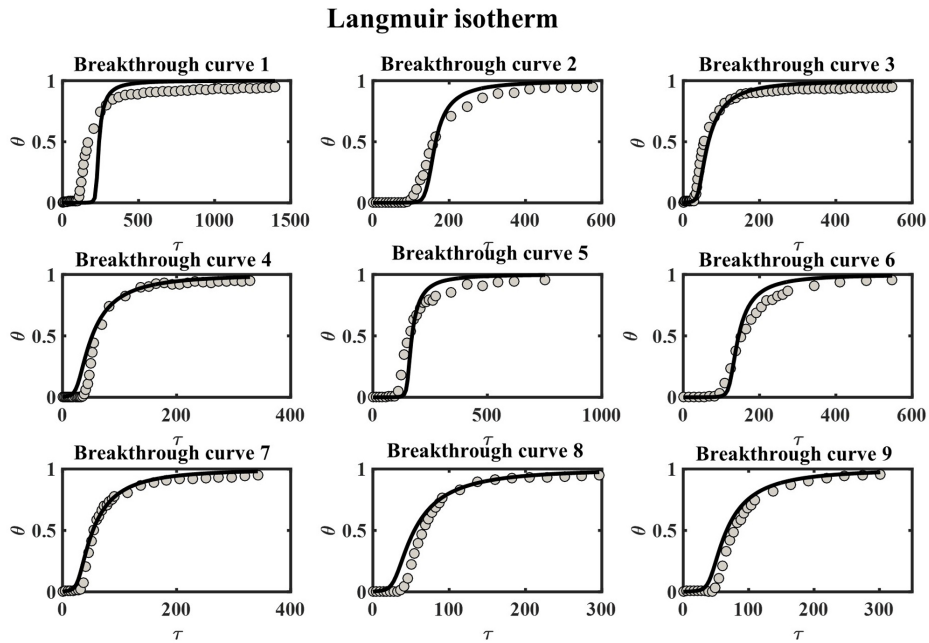


Figure 7. Predicted breakthrough curves obtained using the Langmuir isotherm coupled to the mass balance model.

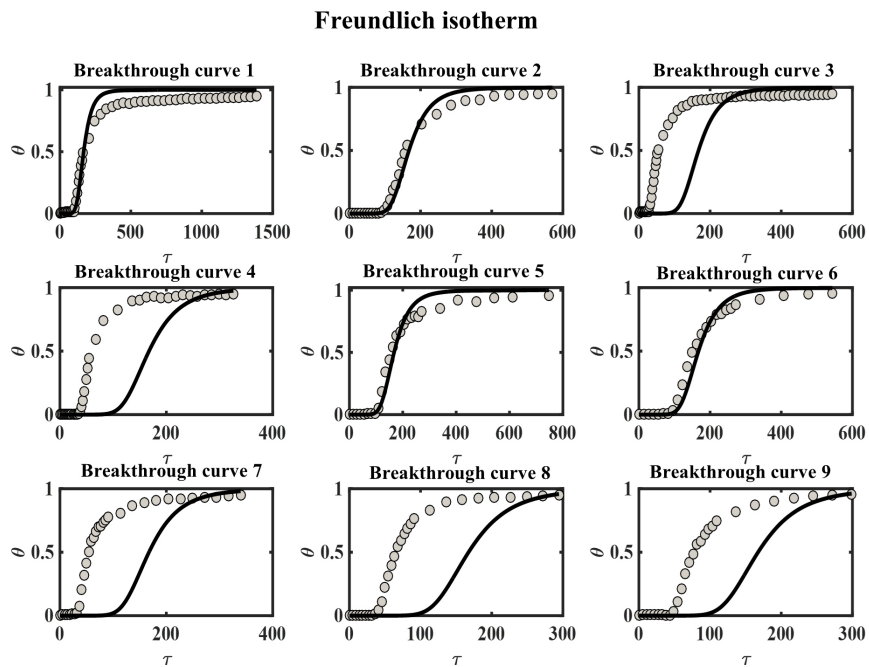


Figure 8. Predicted breakthrough curves obtained using the Freundlich isotherm coupled to the mass balance model.

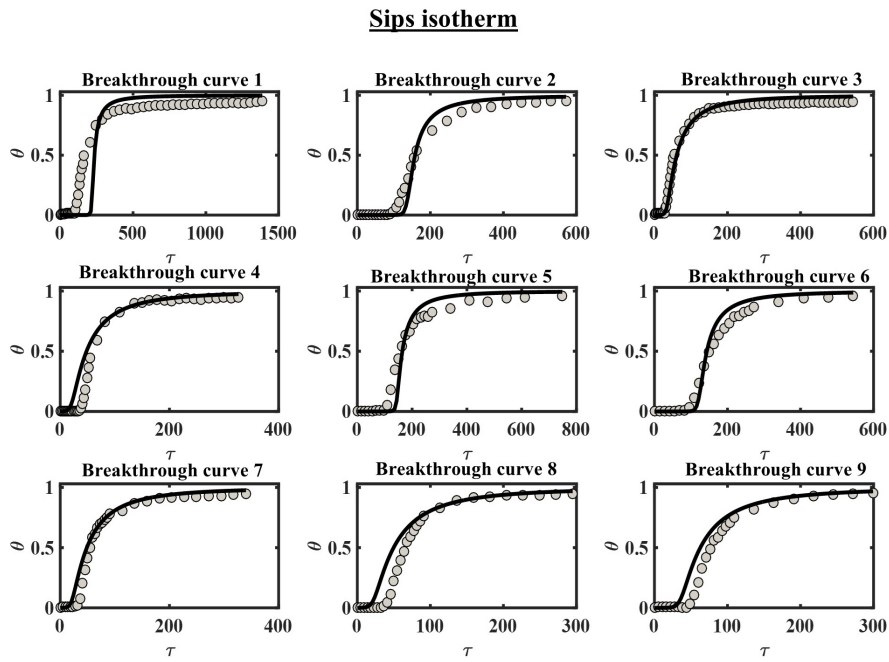


Figure 9. Predicted breakthrough curves obtained using the Sips isotherm coupled to the mass balance model.

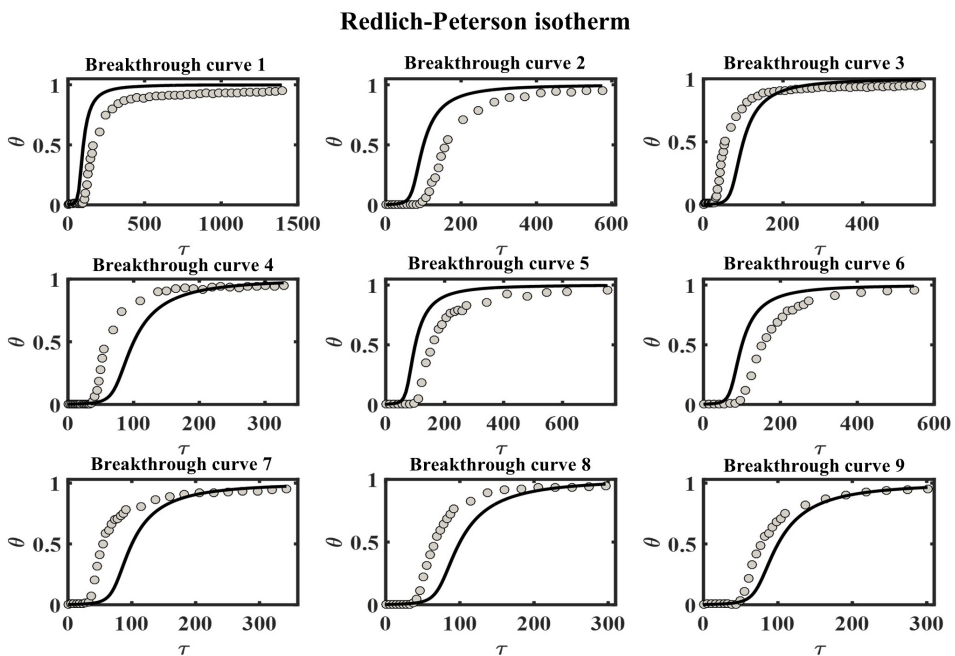


Figure 10. Predicted breakthrough curves obtained using the Redlich-Peterson isotherm coupled to the mass balance model.

For the model coupled with the Freundlich isotherm (Fig. 8), only the predicted breakthrough curves 1, 2, 5 and 6 reasonably approximated the experimental data. In most cases analyzed with this isotherm, the predictions were far from the experimental data, as can be seen in the Supplementary Material of this work. Therefore, the Freundlich isotherm does not provide the best basis for predicting the scenarios in the present study.

The Redlich-Peterson isotherm (Fig. 10) was also not the most suitable for predicting the adsorption breakthrough curves of DCF on activated charcoal. Only case 3 (Supplementary Material) achieved good predictions of breakthrough curves that were not used in the probability calculation.

CONCLUSIONS

The adsorption of the drug diclofenac sodium (DCF) on granulated activated charcoal was studied experimentally and numerically. A mass balance-based model was used to describe the continuous phenomenon in a fixed bed column. This problem was approached using Bayesian statistics so that the experimental uncertainties could be considered, and the Markov chain Monte Carlo (MCMC) method was used to estimate the parameters of interest.

The individual estimates of the nine breakthrough curves were in general satisfactory, especially for the coupling between the model and the Sips isotherm, which came closest to the experimental data. The Bayesian BIC metric confirmed what was observed graphically, indicating that the coupling with the Sips isotherm was the most likely to represent the real phenomenon of sodium diclofenac adsorption on activated carbon.

The different operating conditions C_0 , W and Q have been shown to influence not only the experimental performance of adsorption in the fixed bed column, but also the process of parameter estimation and scenario prediction. This influence had already been observed in a previous publication by de Franco (2018) who showed that increasing the initial concentration C_0 and decreasing the feed flow rate Q resulted in an increase in the amount of diclofenac adsorbed on the column.

The model and the MCMC method were effective in predicting different scenarios based on data available from other experimental conditions. This indicates that prediction is an advantageous application of modeling, since it promotes a reduction in the number of repetitions needed to analyze the behavior of the phenomenon when only the operating conditions of the system are varied, as well as contributing to a reduction in costs and time invested in data acquisition.

The GDF model is a simple and effective alternative to more complex models applied for the same purpose. The possibility of the gamma exponent γ not being restricted to a fixed value, but varying within a range, can facilitate not only an adequate fit to the data, but also scaling up.

Nomenclature

- C Adsorbate concentration in the liquid phase (mg L^{-1})
- C_0 Initial adsorbate concentration (mg L^{-1})
- C_{eq} Solute concentration at equilibrium (mg L^{-1})
- \bar{q} Adsorbate concentration in the solid phase (mg g^{-1})
- u_0 Interstitial velocity (cm min^{-1})
- D_z Axial dispersion coefficient ($\text{cm}^2 \text{min}^{-1}$)
- k_L Langmuir isotherm constant (L mg^{-1})
- k_F Freundlich isotherm constant ($(\text{mg g}^{-1})/(\text{L mg}^{-1})^{1/n}$)
- k_{Sips} Sips isotherm constant (L mg^{-1})
- k_{RP} Redlich-Petersen isotherm constant (L mg^{-1})
- b Parameter of the Redlich-Petersen isotherm ($0 \leq b \leq 1$)
- a Parameter of the Redlich-Petersen isotherm ($\text{L}^b \text{mg}^b$)
- q_{max} Maximum column adsorption capacity (mg g^{-1})
- k_s Global mass transfer coefficient (min^{-1})
- k_{QDF} Quadratic driving force constant ($\text{kg g}^{-1} \text{min}^{-1}$)
- q^* Equilibrium concentration in the solid phase (mg g^{-1})
- ϵ_L Porosity
- t Time (min)
- ρ_L Bed specific density (g L^{-1})
- θ Dimensionless concentration of adsorbate at the exit of the bed
- Pe Péclet number
- η Dimensionless column length
- τ Dimensionless time
- γ Gamma exponent (adm)

Acknowledgments

We are grateful for the financial support provided by PROPESP/UFGA (PAPQ, process number 23073.069855/2022-11) and FAPESPA (process number 013/2022) via project titled "Adsorção de gases em leito fixo: Uso de adsorventes produzidos a partir de resíduos de mineração em Sistema com escala semi piloto" for the publication of this article. We express our heartfelt gratitude to Coordenação de Aperfeiçoamento de Pessoal de Nível Superior (CAPES), Conselho Nacional de Desenvolvimento Científico e Tecnológico (CNPq), and Financiadora de Estudos e Projetos (FINEP) for the financial support provided, enabling our research and academic contributions.

REFERENCES

- ACUÑA V, GINEBRED A, MOR J, PETROVIC M, SABATER S, SUMPTER J & BARCELÓ D. 2015. Balancing the health benefits and environmental risks of pharmaceuticals: Diclofenac as an example. *Envir Int* 85: 327-333.
- AGÊNCIA NACIONAL DE VIGILÂNCIA SANITÁRIA. 2021. Anuário Estatístico do Mercado Farmacêutico.
- AHMED M & HAMEED B. 2018. Removal of emerging pharmaceutical contaminants by adsorption in a fixed-bed column: a review. *Ecotoxicol Envir Safety* 149: 257-266.
- AMADOR ICB, NUNES KGP, DE FRANCO MAE, VIEGAS BM, MACÊDO EN, FÉRIS LA & ESTUMANO DC. 2022. Application of Approximate Bayesian Computational technique to characterize the breakthrough of paracetamol adsorption in fixed bed column. *Int Comm Heat Mass Transf* 132: 105917.
- AMALINA F, ABD RAZAK AS, KRISHNAN S, ZULARISAM A & NASRULLAH M. 2022. A comprehensive assessment of the method for producing biochar, its characterization, stability, and potential applications in regenerative economic sustainability—a review. *Cleaner Mat* 3: 100045.
- AMÉRICO-PINHEIRO JHP ET AL. 2022. Effective adsorption of diclofenac and naproxen from water using fixed-bed column loaded with composite of heavy sugarcane ash and polyethylene terephthalate. *Envir Res* 211: 112971.
- AVCU T, ÜNER O & GEÇGEL Ü. 2021. Adsorptive removal of diclofenac sodium from aqueous solution onto sycamore ball activated carbon—isootherms, kinetics, and thermodynamic study. *Surf Interf* 24: 101097.
- AYAWEI N, EBELEGI AN, WANKASI D ET AL. 2017. Modelling and interpretation of adsorption isotherms. *J Chem* 2017: 3039817.
- BRANDANI S. 2021. Kinetics of liquid phase batch adsorption experiments. *Adsorption* 27(3): 353-368.
- CARDOSO AC, DIAS CS, MOURA CHR, FERREIRA JL, RODRIGUES EC, MACÊDO EN, ESTUMANO DC & VIEGAS BM. 2023. Use of Bayesian Methods in the Process of Uranium Bioleaching by *Acidithiobacillus ferrooxidans*. *Appl Sci* 14(1): 109.
- CHEN X, HOSSAIN MF, DUAN C, LU J, TSANG YF, ISLAM MS & ZHOU Y. 2022. Isotherm models for adsorption of heavy metals from water—A review. *Chemosphere* 307: 135545.
- CUCCARESE M, BRUTTI S, DE BONIS A, TEGHIL R, MANCINI IM, MASI S & CANIANI D. 2021. Removal of diclofenac from aqueous solutions by adsorption on thermo-plasma expanded graphite. *Sci Rep* 11(1): 3427.
- DA SILVA MEDEIROS DCC, CHELME-AYALA P & EL-DIN MG. 2023. Sludge-based activated biochar for adsorption treatment of real oil sands process water: Selectivity of naphthenic acids, reusability of spent biochar, leaching potential, and acute toxicity removal. *Chem Eng J* 463: 142329.
- DANCKWERTS PV. 1995. Continuous flow systems. Distribution of residence times. *Chem Eng Sci* 50(24): 3857-3866.
- DANG C, SUN F, JIANG H, HUANG T, LIU W, CHEN X & JI H. 2020. Pre-accumulation and in-situ destruction of diclofenac by a photo-regenerable activated carbon fiber supported titanate nanotubes composite material: Intermediates, DFT calculation, and ecotoxicity. *J Hazard Mat* 400: 123225.
- DE FRANCO MAE, DE CARVALHO CB, BONETTO MM, DE PELEGRINI SOARES R & FÉRIS LA. 2018. Diclofenac removal from water by adsorption using activated carbon in batch mode and fixed-bed column: isotherms, thermodynamic study and breakthrough curves modeling. *J Clean Prod* 181: 145-154.
- DEEMTER D, OLLER I, AMAT AM & MALATO S. 2021. Effect of salinity on preconcentration of contaminants of emerging concern by nanofiltration: Application of solar photo-Fenton as a tertiary treatment. *Sci Total Environ* 756: 143593.
- DONG M, HE L, JIANG M, ZHU Y, WANG J, GUSTAVE W, WANG S, DENG Y, ZHANG X & WANG Z. 2023. Biochar for the removal of emerging pollutants from aquatic systems: a review. *Int J Environ Res Public Health* 20(3): 1679.
- ELABADSA M, VARGA M & MIHUCZ VG. 2019. Removal of selected pharmaceuticals from aqueous matrices with activated carbon under flow conditions. *Microchemical Journal* 150: 104079.
- FERREIRA JR, SENNA AP, MACÊDO EN & ESTUMANO DC. 2023. Aerobic bioreactors: A Bayesian point of view applied to hydrodynamic characterization and experimental evaluation of tracers. *Chem Eng Sci* 277: 118850.
- GAMERMAN D & LOPES HF. 2006. Markov chain Monte Carlo: stochastic simulation for Bayesian inference. Chapman and Hall/CRC.
- GEANKOPLIS C. 1993. Transport Processes and Unit Operations, 3 Prentice-Hall International Inc. New Jersey, p. 144-145.
- HAAP T, TRIEBSKORN R & KÖHLER HR. 2008. Acute effects of diclofenac and DMSO to *Daphnia magna*: immobilisation and hsp70-induction. *Chemosphere* 73(3): 353-359.
- HARO NK, DÁVILA IVJ, NUNES KGP, DE FRANCO MAE, MARCILIO NR & FÉRIS LA. 2021. Kinetic, equilibrium and thermodynamic studies of the adsorption of paracetamol in activated carbon in batch model and fixed-bed column. *Appl Water Sci* 11: 1-9.
- HIEW BYZ, LEE LY, LAI KC, GAN S, THANGALAZHY-GOPAKUMAR S, PAN GT & YANG TCK. 2019. Adsorptive decontamination of diclofenac by three-dimensional graphene-based adsorbent: response surface methodology, adsorption equilibrium, kinetic and thermodynamic studies. *Envir Res* 168: 241-253.

- HOEGER B, KÖLLNER B, DIETRICH DR & HITZFELD B. 2005. Water-borne diclofenac affects kidney and gill integrity and selected immune parameters in brown trout (*Salmo trutta f. fario*). *Aquatic Toxicol* 75(1): 53-64.
- HUANG C, LIANG R, LIU F, YANG H & LIN X. 2022. Effect of dimensionless heat input during laser solid forming of high-strength steel. *J Mat Sci Technol* 99: 127-137.
- JEMUTAI-KIMOSOP S, OKELLO VA, SHIKUKU VO, ORATA F & GETENGA ZM. 2022. Synthesis of mesoporous akaganeite functionalized maize cob biochar for adsorptive abatement of carbamazepine: Kinetics, isotherms, and thermodynamics. *Cleaner Mat* 5: 100104.
- JUELA D, VERA M, CRUZAT C, ALVAREZ X & VANEGAS E. 2021. Mathematical modeling and numerical simulation of sulfamethoxazole adsorption onto sugarcane bagasse in a fixed-bed column. *Chemosphere* 280: 130687.
- JURADO-DAVILA V, DE OLIVEIRA JT, ESTUMANO D & FÉRIS LA. 2023a. Fixed-bed column for phosphate adsorption combining experimental observation, mathematical simulation, and statistics: Classical and Bayesian. *Separat Purificat Technol* 317: 123914.
- JURADO-DAVILA IV, SCHNEIDER IAH, ESTUMANO D & AMARAL FÉRIS L. 2023b. Phosphate removal using dolomite modified with ultrasound: mathematical and experimental analysis. *J Environ Sci Health, Part A* 58(5): 469-482.
- KAPIO J & SOMERSALO E. 2006. Statistical and computational inverse problems. Vol. 160. Springer Science & Business Media.
- KALAM S, ABU-KHAMSIN SA, KAMAL MS & PATIL S. 2021. Surfactant adsorption isotherms: A review. *ACS Omega* 6(48): 32342-32348.
- KAMARUDIN NS, DAHALAN FA, HASAN M, AN OS, PARMIN NA, IBRAHIM N, HAMDZAH M, ZAIN NAM, MUDA K & WIKURENDRA EA. 2022. Biochar: A review of its history, characteristics, factors that influence its yield, methods of production, application in wastewater treatment and recent development. *Biointerface Res Appl Chem* 12(6): 7914-7926.
- KUMAR H, KUMAR S, GNANASEKARAN N & BALAJI C. 2018. A markov chain monte Carlo-Metropolis hastings approach for the simultaneous estimation of heat generation and heat transfer coefficient from a teflon cylinder. *Heat Transfer Eng* 39(4): 339-352.
- LAI L, TEH L, TIMMIATI S, KAMARUDIN N & SETIABUDI H. 2023. A sustainable solution for diclofenac adsorption: Chitosan-modified fibrous silica KCC-1 adsorbent. *J Environ Chem Eng* 11(6): 111295.
- LI Z, YAHYAOU S, BOUZID M, ERTO A & DOTTO GL. 2021. Interpretation of diclofenac adsorption onto ZnFe₂O₄/chitosan magnetic composite via BET modified model by using statistical physics formalism. *J Molec Liquid* 327: 114858.
- LONAPPAN L, BRAR SK, DAS RK, VERMA M & SURAMPALLI RY. 2016. Diclofenac and its transformation products: environmental occurrence and toxicity-a review. *Envir Int* 96: 127-138.
- LONAPPAN L, ROUISSI T, LIU Y, BRAR SK & SURAMPALLI R. 2019. Removal of diclofenac using microbiocchar fixed-bed column bioreactor. *J Environ Chem Eng* 7(1): 102894.
- LV Y ET AL. 2021. Efficient adsorption of diclofenac sodium in water by a novel functionalized cellulose aerogel. *Environ Res* 194: 110652.
- MARTINS Y, ALMEIDA A, VIEGAS B, DO NASCIMENTO R & RIBEIRO NDP. 2020. Use of red mud from amazon region as an adsorbent for the removal of methylene blue: process optimization, isotherm and kinetic studies. *Int J Environ Sci Technol* 17: 4133-4148.
- MIRZAE SA, BAYATI B, VALIZADEH MR, GOMES HT & NOORIMOTLAGH Z. 2021. Adsorption of diclofenac on mesoporous activated carbons: Physical and chemical activation, modeling with genetic programming and molecular dynamic simulation. *Chem Eng Res Design* 167: 116-128.
- MÓDENES AN, BAZARIN G, BORBA CE, LOCATELLI PPP, BORSATO FP, PAGNO V, PEDRINI R, TRIGUEROS DEG, ESPINOZA-QUIÑONES FR & SCHEUFELE FB. 2021. Tetracycline adsorption by tilapia fish bone-based biochar: Mass transfer assessment and fixed-bed data prediction by hybrid statistical-phenomenological modeling. *J Clean Prod* 279: 123775.
- MOURA CH, VIEGAS BM, TAVARES M, MACEDO E & ESTUMANO DC. 2022. Estimation Of Parameters And Selection Of Models Applied To Population Balance Dynamics Via Approximate Bayesian Computational. *J Heat Mass Transf Res* 9(1): 53-64.
- MOURA CH, VIEGAS BM, TAVARES MR, MACÉDO EN, ESTUMANO DC & QUARESMA JN. 2021. Parameter Estimation in Population Balance through Bayesian Technique Markov Chain Monte Carlo. *J Appl Comput Mechanic* 7(2): 890-901.
- NADOUR M, BOUKRAA F & BENABOURA A. 2019. Removal of Diclofenac, Paracetamol and Metronidazole using a carbon-polymeric membrane. *J Environ Chem Eng* 7(3): 103080.
- NUNES KGP, DÁVILA IVJ, AMADOR ICB, ESTUMANO DC & FÉRIS LA. 2021. Evaluation of zinc adsorption through batch and continuous scale applying Bayesian technique for estimate parameters and select model. *J Environ Sci Health, Part A* 56(11): 1228-1242.
- NUNES KGP, DAVILA IVJ, ARNOLD D, MOURA CHR, ESTUMANO DC & FÉRIS LA. 2022. Kinetics and thermodynamic study of laponite application in caffeine removal by adsorption. *Environ Process* 9(3): 47.
- OKPARA OG, OGBEIDE OM, IKE OC, MENECHUKWU KC & EJIKE EC. 2021. Optimum isotherm by linear and nonlinear regression methods for lead (II) ions adsorption from aqueous solutions

using synthesized coconut shell-activated carbon (SCSAC). *Toxin Rev* 40(4): 901-914.

OTÁLVARO-MARÍN HL & MACHUCA-MARTÍNEZ F. 2021. New approach for the dimensionless analysis of a unidirectional flow solar reactor based on Damköhler's number profiles. *Heliyon* 7(5).

PEREIRA AM, SILVA LJ, LARANJEIRO CS, MEISEL LM, LINO CM & PENA A. 2017. Human pharmaceuticals in Portuguese rivers: The impact of water scarcity in the environmental risk. *Sci Total Environ* 609: 1182-1191.

PEZOTI O, CAZETTA AL, BEDIN KC, SOUZA LS, MARTINS AC, SILVA TL, JÚNIOR OOS, VISENTAINER JV & ALMEIDA VC. 2016. NaOH-activated carbon of high surface area produced from guava seeds as a high-efficiency adsorbent for amoxicillin removal: Kinetic, isotherm and thermodynamic studies. *Chem Eng J* 288: 778-788.

RUTHVEN DM. 1984. Principles of adsorption and adsorption processes. J Wiley & Sons.

SAADI R, SAADI Z, FAZALI R & FARD NE. 2015. Monolayer and multilayer adsorption isotherm models for sorption from aqueous media. *Korean J Chem Eng* 32: 787-799.

SAARELA T, LAFDANI EK, LAURÉN A, PUMPANEN J & PALVIAINEN M. 2020. Biochar as adsorbent in purification of clear-cut forest runoff water: Adsorption rate and adsorption capacity. *Biochar* 2: 227-237.

SCHEUFELE FB, DA SILVA ES, CAZULA BB, MARINS DS, SEQUINEL R, BORBA CE, PATUZZO GS, LOPEZ TFM & ALVES HJ. 2021. Mathematical modeling of low-pressure H₂S adsorption by babassu biochar in fixed bed column. *J Environ Chem Eng* 9(1): 105042.

SHAKERI F & DEGHAN M. 2008. The method of lines for solution of the one-dimensional wave equation subject to an integral conservation condition. *Comp Math Appl* 56(9): 2175-2188.

SHAMSUDIN MS, AZHA SF, SELLAOUI L, BADAWI M, BONILLA-PETRICIOLET A & ISMAIL S. 2022. Performance and interactions of diclofenac adsorption using Alginate/Carbon-based Films: Experimental investigation and statistical physics modelling. *Chem Eng J* 428: 131929.

SOARES SF, FERNANDES T, SACRAMENTO M, TRINDADE T & DANIEL-DA SILVA AL. 2019. Magnetic quaternary chitosan hybrid nanoparticles for the efficient uptake of diclofenac from water. *Carbohydrate Polymers* 203: 35-44.

TANG Q, QIU C, ZHANG Y, ZHANG X, YUAN Z, TAN H, WANG L, DE HOOP CF, QI J & HUANG X. 2023. Effective Adsorption of Diclofenac Sodium from Wastewater by Nanocellulose/Alum/Chitosan/Polyethyleneimine Biohybrid Aerogel Beads Adsorbent. *J Polymer Environ* 31(3): 1129-1143.

TATARCHUK T, MYSLIN M, LAPCHUK I, SHYICHUK A, MURTHY AP, GARGULA R, KURZYDŁO P, BOGACZ BF & PĘDZIWIATR AT. 2021. Magnesium-zinc ferrites as magnetic adsorbents for Cr (VI) and Ni (II) ions removal: Cation distribution and antistructure modeling. *Chemosphere* 270: 129414.

TAVARES R, SANTANA DIAS C, RODRIGUES MOURA CH, RODRIGUES EC, VIEGAS B, MACEDO E & ESTUMANO DC. 2022. Parameter Estimation in Mass Balance Model Applied in Fixed Bed Adsorption Using the Markov Chain Monte Carlo Method. *J Heat Mass Transf Res* 9(2): 219-232.

TOFFOLI DE OLIVEIRA J, DA LUZ ARSUFU AB, CARDOSO ESTUMANO D & FERIS LA. 2023. Bayesian computational technique for modeling caffeine adsorption in a fixed-bed column: use of the maximum adsorption capacity deterministically and experimental design. *Industr Eng Chem Res* 62(18): 7127-7137.

TOGUE KAMGA F. 2019. Modeling adsorption mechanism of paraquat onto Ayous (*Triplochiton scleroxylon*) wood sawdust. *Appl Water Sci* 9(1): 1.

UNUABONAH EI, OMOROGIE MO & OLADOJA NA. 2019. Modeling in adsorption: fundamentals and applications. In: *Composite nanoadsorbents*. Elsevier, p. 85-118.

VERA M, JUELA DM, CRUZAT C & VANEGAS E. 2021. Modeling and computational fluid dynamic simulation of acetaminophen adsorption using sugarcane bagasse. *J Environ Chem Eng* 9(2): 105056.

VIEGAS BM, MAGALHÃES E, ORLANDE H, ESTUMANO D & MACÊDO E. 2023. Experimental study and mathematical modelling of red mud leaching: application of Bayesian techniques. *Int J Environ Sci Technol* 20(5): 5533-5546.

WANG J & GUO X. 2020. Adsorption isotherm models: Classification, physical meaning, application and solving method. *Chemosphere* 258: 127279.

WU Q ET AL. 2019. Adsorption characteristics of Pb (II) using biochar derived from spent mushroom substrate. *Sci Rep* 9(1): 15999.

ZHANG C, BARRON L & STURZENBAUM S. 2021. The transportation, transformation and (bio) accumulation of pharmaceuticals in the terrestrial ecosystem. *Sci Total Environ* 781: 146684.

ZHAO R, ZHENG H, ZHONG Z, ZHAO C, SUN Y, HUANG Y & ZHENG X. 2021. Efficient removal of diclofenac from surface water by the functionalized multilayer magnetic adsorbent: Kinetics and mechanism. *Sci Total Environ* 760: 144307.

SUPPLEMENTARY MATERIAL

Table S1.
Figure S1-S16.

How to cite

DIAS CS, FRANCO MAE, RODRIGUES EC, FERREIRA JL, VIEGAS BM, FÉRIS LA, ESTUMANO DC & MACÊDO EN. 2024. Diclofenac sodium adsorption on activated carbon: experimental, modeling and bayesian statistics. An Acad Bras Cienc 96: e20231110. DOI 10.1590/0001-3765202420231110.

*Manuscript received on October 13, 2023;
accepted for publication on March 4, 2024*

Macêdo: Conceptualization, methodology, software, validation, writing – review and editing, supervision. All authors have read and agreed to the published version of the manuscript.

**CAMILA S. DIAS¹**

<https://orcid.org/0000-0002-4087-4197>

MARCELA ANDREA E. FRANCO²

<https://orcid.org/0000-0003-3557-0700>

EMERSON C. RODRIGUES³

<https://orcid.org/0000-0002-0303-4578>

JOSIEL L. FERREIRA³

<https://orcid.org/0000-0003-0345-3526>

BRUNO M. VIEGAS⁴

<https://orcid.org/0000-0002-2768-652X>

LILIANA A. FÉRIS⁵

<https://orcid.org/0000-0002-5900-4474>

DIEGO C. ESTUMANO⁴

<https://orcid.org/0000-0003-4318-4455>

EMANUEL N. MACÊDO^{1,3}

<https://orcid.org/0000-0002-4652-8316>

¹Universidade Federal do Pará, Rua Augusto Corrêa, 01, 66075-970 Belém, PA, Brazil

²Universidade Federal do Rio Grande do Sul, Programa de Pós-Graduação em Engenharia Química, Rua Ramiro Barcelos, 2777, 90040-040 Porto Alegre, RS, Brazil

³Universidade Federal do Pará, Faculdade de Engenharia Química, Rua Augusto Corrêa, 01, 66075-970 Belém, PA, Brazil

⁴Universidade Federal do Pará, Faculdade de Biotecnologia, Rua Augusto Corrêa, 01, 66075-970 Belém, PA, Brazil

⁵Universidade Federal do Rio Grande do Sul, Departamento de Engenharia Química, Rua Ramiro Barcelos, 2777, 90040-040 Porto Alegre, RS, Brazil

Correspondence to: **Emanuel N. Macêdo**

E-mail: enegrao@ufpa.br

Author contributions

C. S. Dias: Methodology, software, writing - original draft, investigation, formal analysis, visualization. M. A. E. Franco: Experimental data, conceptualization, writing - review and editing. E. C. Rodrigues, J. L. Ferreira and B. M. Viegas: Methodology, formal analysis, validation, writing - review and editing. L. A. Féris: Methodology, experimental data, formal analysis, writing - review and editing. D. C. Estumano and E. N.